Activated Graphene-Based Carbons as Supercapacitor Electrodes with Macro- and Mesopores

TaeYoung Kim,[†] Gyujin Jung,[‡] Seonmi Yoo,[‡] Kwang S. Suh,[‡,*] and Rodney S. Ruoff[†,*]

[†]Department of Mechanical Engineering and Materials Science and Engineering Program, University of Texas at Austin, One University Station C2200, Austin, Texas 78712, United States and [‡]Department of Materials Science and Engineering, Korea University, 5-1 Anam-dong, Seongbuk-gu, Seoul 136-713, Republic of Korea

ABSTRACT Electric double layer capacitors (or supercapacitors) store charges through the physisorption of electrolyte ions onto porous carbon electrodes. The control over structure and morphology of carbon electrode materials is therefore an effective strategy to render them high surface area and efficient paths for ion diffusion. Here we demonstrate the fabrication of highly porous graphene-derived carbons with hierarchical pore structures in which mesopores are integrated into macroporous scaffolds. The macropores were introduced by assembling graphene-based hollow spheres, and the mesopores were derived from the chemical activation with potassium hydroxide. The unique three-dimensional pore structures in the produced graphene-derived carbons give rise to a Brunauer–Emmett–Teller surface area value of up to 3290 $m^2 g^{-1}$ and provide an efficient pathway for electrolyte ions to diffuse into the interior surfaces of bulk electrode particles. These carbons exhibit both high gravimetric (174 F g^{-1}) and volumetric (~100 F cm^{-3}) specific capacitance in an ionic liquid electrolyte in acetonitrile. The energy density and power density of the cell assembled with this carbon electrode are also high, with gravimetric values of 74 Wh kg^{-1} and 338 kW kg^{-1} and volumetric values of 44 Wh L^{-1} and 199 kW L^{-1}, respectively. The supercapacitor performance achieved with these graphene-derived carbons is attributed to their unique pore structure and makes them potentially promising for diverse energy storage devices.

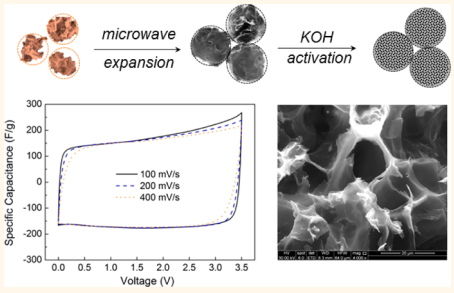

KEYWORDS: graphene-derived carbon · hierarchical pore structure · specific surface area · supercapacitors · electrical double layer capacitors

Electrical double layer capacitors (EDLCs), also called supercapacitors, are a class of energy storage devices that store charges in an electric double layer formed through physisorption of electrolyte ions onto porous carbon electrodes.[1−4] With a promising combination of features such as high power density and excellent cycling stability, they are finding uses in applications including high-power electronic devices, uninterruptable power supplies, and electric and hybrid electric vehicles.[1,2,5] However, for most of these practical applications, they suffer from limited energy density which is typically on the order of 4−5 Wh/kg for fully assembled cells, an order of magnitude lower than the batteries.[3] Significant research has been directed toward improving their energy densities by (i) increasing capacitance with high-surface-area carbon electrode materials and (ii) enhancing the operational voltage with electrolytes that possess high potential windows.[6]

As the specific capacitance of supercapacitors is strongly affected by carbon electrodes having a large surface area accessible to electrolyte ions, porous carbon materials such as activated carbon,[3] carbide-derived carbons,[4,7,8] ordered mesoporous carbons,[9,10] carbon aerogels,[11] and carbon nanotubes[12−14] have been studied as high-surface-area electrodes. Graphene-based materials are attractive in this regard as electrode materials for supercapacitors because of their high theoretical surface area (2630 $m^2 g^{-1}$) and electrical conductivity.[15] A variety of graphene-based materials with different chemical structures and morphologies such as chemically modified graphene,[16] microwave-expanded graphite oxide (MEGO),[17] and curved graphene[18] have been explored as electrode materials for supercapacitors. More recently, a graphene-derived carbon with extremely high surface area of up to ~3100 $m^2 g^{-1}$ has been reported, which was prepared by microwave irradiation of

* Address correspondence to r.ruoff@mail.utexas.edu (Rodney S. Ruoff); suhkwang@korea.ac.kr (Kwang S. Suh).

Received for review April 25, 2013 and accepted July 7, 2013.

Published online July 07, 2013
10.1021/nn402077v

© 2013 American Chemical Society

graphite oxide (GO) followed by chemical activation with potassium hydroxide (KOH).[19] This activated microwave-expanded graphite oxide (a-MEGO) has a large fraction of micro- and mesopores that provide a large and accessible surface area for charge accommodation and therefore improved specific capacitance in organic and ionic liquid electrolytes to achieve a relatively high gravimetric energy density.[19,20]

However, most graphene-derived carbons have a surface area likely exploited only to a limited degree, presumably because they may form stacked agglomerates during processing and thus may have limited ion diffusion paths inside some narrow channels.[21] If such graphene platelets are assembled in a way that has a hierarchical porous architecture by achieving mesopores within interconnected macroporous scaffolds,[22,23] it could offer potential structural advantages in that electrolyte ions can diffuse to the interior surface efficiently for extensive EDL formation over larger accessible surfaces, potentially leading to more effective energy storage devices. Herein, we present the fabrication of hierarchically porous graphene-derived carbons with meso- and macropores through chemical activation of graphene-based hollow carbon spheres.

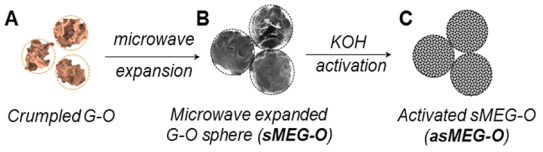

Scheme 1. Schematic of the fabrication of highly porous graphene-derived carbons with hierarchical pore structures: (A) graphene oxide (G-O) sheets are transformed into crumpled ball-like G-O particles by aerosol spray drying technique, (B) under microwave irradiation, crumpled G-O particles form hollow graphene-based spheres, and (C) chemical activation with potassium hydroxide.

RESULTS AND DISCUSSION

The synthesis is schematically illustrated in Scheme 1. First, graphene oxide (G-O) was formed into crumpled ball-like particles by aerosol spray drying,[18,24] which involved suspension of G-O into the fine droplets that during evaporation transformed the G-O sheets into crumpled and hollow G-O particles. These G-O particles were then treated in a microwave oven, which led to a degree of deoxygenation and a large volume expansion to yield black and fluffy powders composed of hollow spheres of microwave-expanded G-O (denoted as sMEG-O). Following the irradiation with a microwave, the sMEG-O powders were placed on a poly(tetrafluoroethylene) (PTFE) membrane filter and infiltrated by a KOH aqueous solution under vacuum-assisted directional flow. The resulting sMEG-O/KOH mixture was dried and then heated in a tube furnace under argon flowing at 800 °C for 1 h and a pressure of 1 atm, yielding activated microwave-expanded G-O spheres denoted as asMEG-O (see Experimental Section for further details of material preparation).

The morphologies of the graphene-derived carbons produced in each step were examined by scanning electron microscopy (SEM). SEM images showed that G-O particles prepared by the aerosol spray drying method ranged in size from 1 to 4 μm and had a highly crumpled morphology (Figure 1A).[25] Microwave-expanded G-O spheres (sMEG-O) were 3 to 10 μm in diameter with relatively smooth and flat surfaces, presumably due to the expansion of the crumpled G-O particles caused by rapid microwave heating

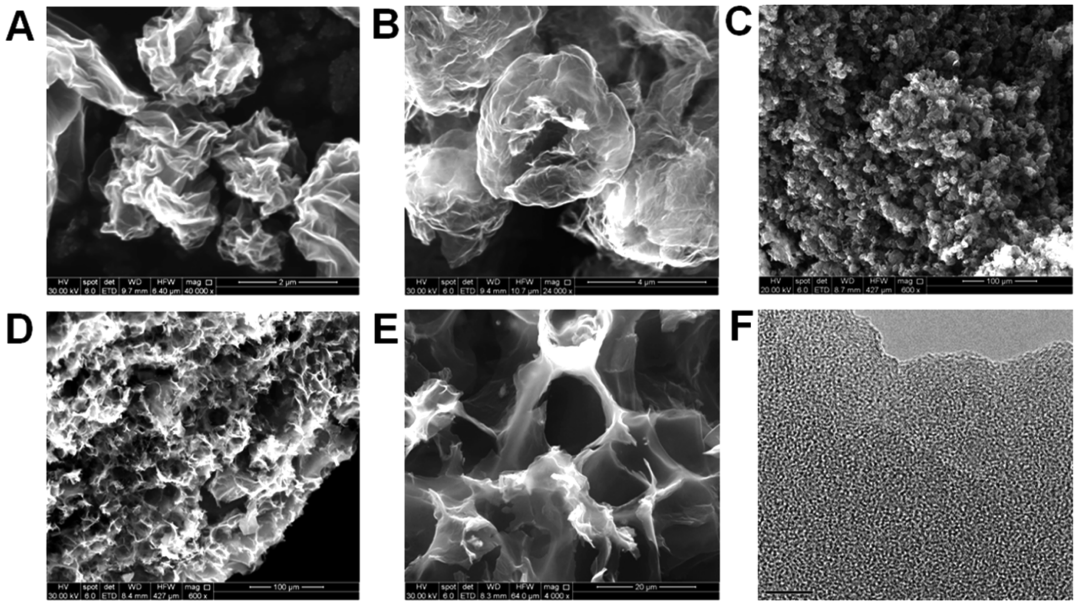

Figure 1. SEM micrographs of (A) crumpled G-O particles, (B, C) hollow spheres of microwave-expanded G-O (sMEG-O), and (D, E) activated sMEG-O (asMEG-O). (F) TEM image of asMEG-O showing the presence of micro- and mesopores (scale bar: 10 nm).

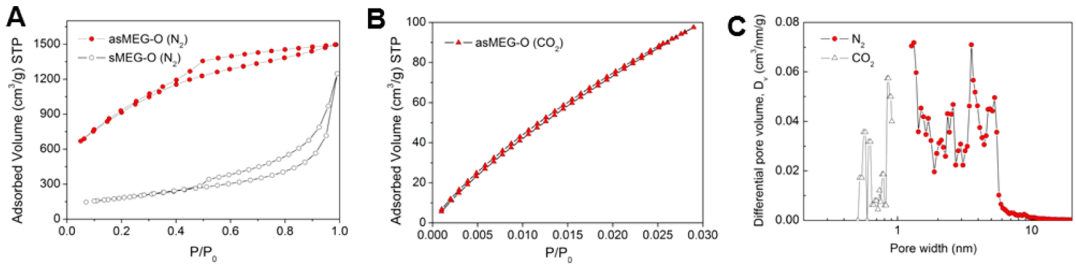

Figure 2. (A) N_2 sorption isotherms (77 K) on sMEG-O and asMEG-O, (B) CO_2 sorption isotherms of asMEG-O (273 K), and (C) pore size distribution of asMEG-O for N_2 (calculated by using a slit/cylinder hybrid NLDFT model) and CO_2 (calculated by using a slit pore NLDFT model).

(Figure 1B and C). SEM images of the activated microwave-expanded G-O spheres (asMEG-O) showed the presence of open, interconnected macropores in a three-dimensional framework (Figure 1D and E). This macroporous structure is attributed to the vacuum-assisted infiltration of KOH solution into the sMEG-O, which causes the sMEG-O to self-assemble into densely packed particles (probably by capillary forces) while preserving the spherical shape of the sMEG-O. High-resolution transmission electron microscopy (TEM) (Figure 1F) also revealed that the asMEG-O had a highly porous carbon structure with a large fraction of micro- and mesopores, very similar to that previously observed in activated graphene (*i.e.*, a-MEGO).[19] In this carbon, macropores are present due to the hollow sMEG-O, while mesopores are introduced by KOH activation of sMEG-O. The overall structure consists of small mesopores within an interconnected macroporous network, which is expected to provide high permeability to electrolyte ions.

The elemental analysis revealed that asMEG-O contain 93.58 wt % C, 0.25 wt % H, and 2.84 wt % O, indicating a low content of H and a high C/O atomic ratio of 43.9 (Table S1). X-ray photoelectron spectroscopy analysis further indicated the presence of a significant fraction of sp^2 carbons and high C/O ratio (Figure S1).

The porosity of asMEG-O carbons was analyzed by N_2 gas adsorption−desorption measurements, and Figure 2A exhibits a characteristic type-IV isotherm with a pronounced hysteresis in the P/P_0 range 0.4−1.0, implying the presence of a large number of mesopores in asMEG-O. In addition, CO_2 adsorption−desorption was performed to assess micropores (pores less than 1 nm) in the low-pressure region (Figure 2B). The pore size calculated by the nonlocal density functional theory (NLDFT) method[26] assuming a slit geometry for micropores and a cylindrical pore geometry for the mesopores indicates the existence of well-defined micro- and mesopores with sizes of less than 10 nm (Figure 2C). Brunauer−Emmett−Teller analysis indicated that the specific surface area of asMEG-O was up to 3290 $m^2\ g^{-1}$ calculated in the P/P_0 range 0.1−0.3, which is much higher than those of unactivated sMEG-O (~650 $m^2\ g^{-1}$, Figure 2A) and even higher than the theoretical limit of graphene itself or values reported for a-MEGO.[19]

Given the highly porous features of asMEG-O, its electrochemical performance as an electrode for supercapacitors was evaluated. Using the best practice method,[27] a two-electrode symmetrical cell was constructed with an asMEG-O electrode and ionic liquid electrolytes such as 1-ethyl-3-methylimidazolium bis-(trifluorosulfonyl)imide, [EMIM][TFSI], and 1-butyl-3-methylimidazolium tetrafluoroborate, [BMIM][BF_4], in acetonitrile. Figure 3 shows the electrochemical performance analyzed through cyclic voltammetry (CV), galvanostatic charge/discharge, and electrochemical impedance spectroscopy for the device made with a combination of asMEG-O electrode and [EMIM]-[TFSI] electrolyte.

The CV profiles were obtained for the voltage sweeps from 0 to 2.7 (Figure S2) and 3.5 V (Figure 3A) with a series of scan rates from 100 to 400 mV s^{-1}. The CV curves are rectangular in shape from 0 to 3.5 V and display similar capacitance values over a wide range of scan rates, indicating a near-ideal capacitive behavior with good rate performance. The charge−discharge curves (Figure 3B) at different current density show good symmetry and nearly linear slopes, which is indicative of efficient EDL formation. In addition, the voltage drop at the beginning of the discharge curve is 0.07 V for the current density of 4.2 A g^{-1}, indicating a device with a relatively low equivalent series resistance (ESR) (4.2 Ω). From the discharge curve, the specific capacitance was calculated as 173, 174, and 174 F g^{-1} at current densities of 2.1, 4.2, and 8.4 A g^{-1}, respectively. The asMEG-O electrodes were also tested in [BMIM][BF_4]/AN electrolyte (AN = acetonitrile), which yielded a similar result with a capacitance of 167 F/g at 2.1, 4.2, and 8.4 A g^{-1} and an ESR of 5.7 Ω (Figure S3). These capacitance values are higher than those of commercially used activated carbons (AC)[3] and comparable to or even higher than the best reported values for other porous carbon-based electrode materials.[19] We attribute this high capacitance value to the hierarchically porous structure of asMEG-O, which facilitates electrolyte ions accessing the interior surfaces of the electrode and leads to an increased charge storage. The electrode density of asMEG-O was estimated to be

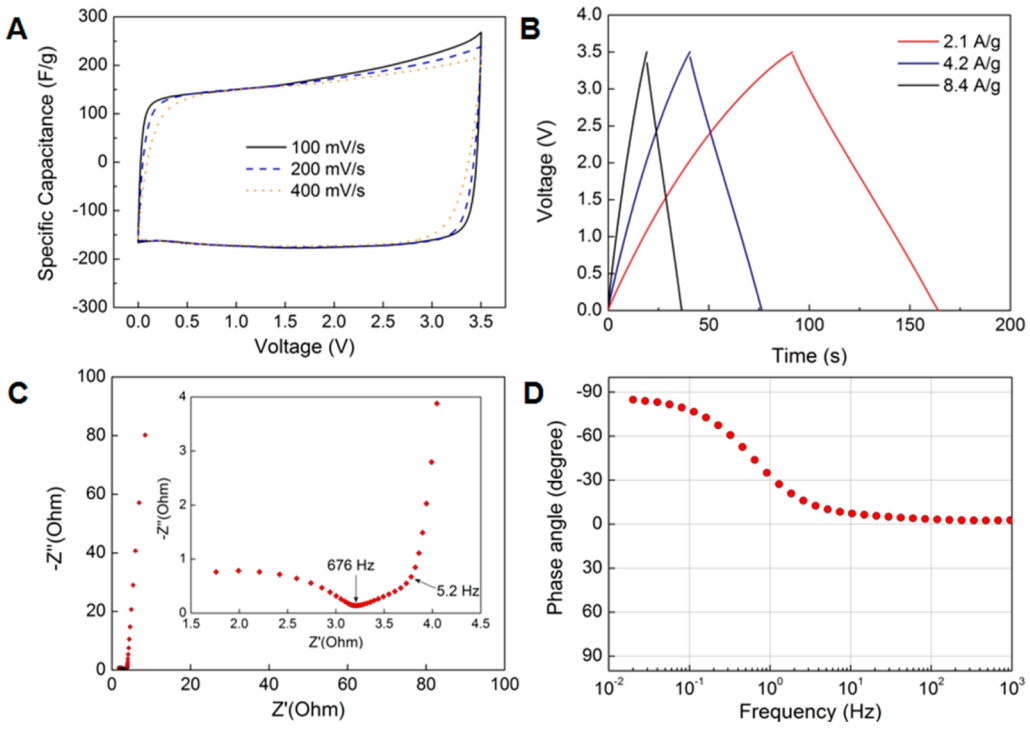

Figure 3. Electrochemical characterization of asMEG-O in [EMIM][TFSI]/AN electrolyte. (A) Cyclic voltammetry curves for different scan rates. (B) Galvanostatic charge/discharge curves under different constant currents. (C) Nyquist plot showing the imaginary part *versus* the real part of impedance. Inset magnifies the data in the high-frequency range. (D) Impedance phase angle *versus* frequency.

0.59 g cm^{-3}, which is higher than that of other activated graphene-based carbons (typically less than 0.4 g cm^{-3}) and close to the bulk densities of activated carbons (~0.5 g cm^{-3}). The corresponding volumetric capacitance was over 100 F cm^{-3}, which is among the best reported for those of activated graphene-based carbons.[19] These results suggest the importance of integrating micro- and mesopores into macroporous scaffolds to improve the electrochemical performance quoted on both a gravimetric and volumetric basis. Figure 3C shows a Nyquist plot obtained for asMEG-O in [EMIM][TFSI]/AN electrolyte in the frequency range of 0.01 Hz to 100 kHz, and a magnified view of the high-frequency region is in the inset. The device displays a nearly ideal capacitive behavior with a vertical slope at the low-frequency region. A resistance of 3.75 Ω obtained by extrapolating the vertical portion of the plot to the real axis confirmed a low ESR value of the device, while a transition between the RC semicircle and the ion diffusion/transport regime was observed at a frequency of 676 Hz, corresponding to a resistance of 3.2 Ω. Figure 3D shows the dependence of phase angle on the frequency. The phase angle is close to −90° at low frequencies, indicating a capacitive behavior, and it reached −45° at the frequency of 0.6 Hz (f_0), giving the corresponding time constant (τ_0) of 1.67 s for the device.[21,28]

The electrochemcial performance of the asMEG-O in the neat [EMIM][TFSI] electrolyte was also tested, and the measured gravimetric capacitance at 3.5 V and a current density of 2 A g^{-1} is 172 F g^{-1} (Figure S4). However, the rate performance is not as good as those from asMEG-O in [EMIM][TFSI]/AN electrolyte, which is likely due to the slow diffusion of electrolyte ions in the neat ionic liquid. The cycling test of the cells also shows ~94% capacitance retention over 1000 cycles at a current density of 2 A g^{-1}, indicating a good stability of the cell (Figure S5).

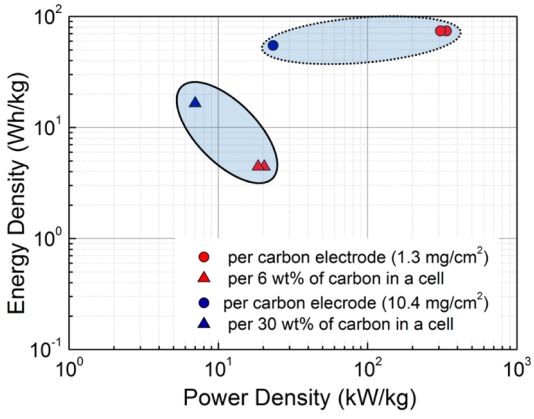

Figure 4. Ragone plots showing energy density and power density. The energy density and power density were normalized to the mass of two electrodes (dotted envelope) and the total mass of the fully assembled cell (solid envelope) based on an assumed value of 6 wt % (red color) and 30 wt % (blue color) for the electrode materials in a packaged commercial cell.

The overall performance of the supercapacitor using asMEG-O as the electrode and ionic liquid electrolytes

is shown in a Ragone plot (Figure 4). Benefitting from a high specific capacitance of up to 174 F/g (obtained with [EMIM][TFSI]/AN electrolyte at a current density of 4.2 A/g) and an operating voltage of 3.5 V, the device exhibited the highest gravimetric energy density of ~74 Wh kg^{-1} and a gravimetric power density of 338 kW kg^{-1} based on the weight of active carbon materials. It is noted that as the electrode thickness increased to 230 μm with the carbon mass loading of 10.4 mg cm^{-2}, the capacitance decreased from 173 to 129 F g^{-1} at a current density of 1.1 A g^{-1} with an increased ESR of 7.0 Ω (Figure S6), which in turn lowers the energy density and power density values to ~55 Wh kg^{-1} and 23 kW kg^{-1}, respectively.

To extrapolate the energy density and power density values in a packaged cell, we assumed that the carbon weights for the 45 and 230 μm thick electrodes account for about 6 and 30 wt % of the total mass of the packaged commercial cell, respectively.[29] In the Ragone plot, the maximum energy density of ~16.5 Wh kg^{-1} was estimated in an assumed packaged cell, which is about a factor of 3 higher than that of commercial AC-based supercapacitors.[3] The normalized power density was as high as ~20 and ~7 kW kg^{-1} for the cells with electrode thicknesses of 45 and 230 μm, respectively.

Using the density value of 0.59 g cm^{-3} for the asMEG-O electrode, the volumetric energy density and volumetric power density were estimated as ~44 Wh L^{-1} and 210 kW L^{-1} for the electrode, respectively, which are to our knowledge among the highest values for porous carbon electrodes without applying any further electrode densification processing (such as applying high-force mechanical compression).[30]

CONCLUSION

In summary, graphene-derived carbons with a favorable hierarchical pore structure have been made. The resulting carbon composed of activated spherical microwave-expanded graphene oxide (asMEG-O) has a continuous macropore structure punctuated with micropores and an extremely high specific surface area, and this structure yields efficient electric double layer formation over a large surface. The asMEG-O had excellent electrochemical performance in ionic liquid electrolytes in terms of gravimetric and volumetric capacitance, which translates into high energy density and high power density. This hierarchical structure and its very high specific surface area could find use in supercapacitors, batteries, and fuel cells.

EXPERIMENTAL SECTION

Material Preparation. Graphene-derived carbons with macro- and mesoporous structures were prepared by the following steps in sequence: (i) preparation of crumpled and hollow graphene oxide (G-O) structures by a spray drying technique,[18,25] then (ii) microwave irradiation, and then (iii) activation of reduced G-O with potassium hydroxide.

(i) Graphite oxide (GO) powder was prepared by a modified Hummers' method[31] and suspended in water as graphene oxide sheets with a concentration of 5 mg mL^{-1}. This aqueous G-O suspension was fed into a spray dryer, where it was "atomized" into fine droplets by a jet collision nebulizer, and the aerosol was delivered into a cylindrical reactor. This aerosol spray drying yielded crumpled and hollow particles composed of overlapped G-O sheets.

(ii) The synthesis of microwave-expanded graphene oxide spheres (sMEG-O) followed a method previously reported for exfoliating a carbon made by microwave irradiation of graphite oxide.[17] The particles comprising overlapped and crumpled G-O sheets were irradiated in a microwave oven operated at 1100 W for 40 s, which resulted in the partial deoxygenation of the G-O particles accompanied by a large volume expansion yielding a sphere-like morphology with rather smooth and flat surfaces.

(iii) The KOH activation process is similar to that previously used on a different precursor carbon.[19] Briefly, 400 mg of sMEG-O powder was placed on a PTFE membrane filter (Sterlitech, 1 μm) and infiltrated with 40 mL of 3.5 M KOH aqueous solution under vacuum-assisted directional flow. The resulting sMEG-O/KOH mixture was dried at 120 °C under vacuum for 24 h and then placed in an alumina boat in a tube furnace under Ar flowing at the rate of 120 sccm and heated to 800 °C according to the following regime: (a) heating from room temperature to 350 °C at a rate of 15 °C/min and 0.5 h heat treatment at 350 °C, (b) heating from 350 to 800 °C at a rate of 5 °C/min and holding the temperature at 800 °C for 1 h, and (c) cooling to room temperature. The activated carbon sample (asMEG-O) was washed with 10% acetic acid solution to remove residual inorganic salts and then an excess of distilled water, followed by drying at 100 °C in an oven for 24 h and annealing at 800 °C in a vacuum for 1 h.

Electrochemical Testing. The asMEG-O powder was mixed with poly(tetrafluoroethylene) (60 wt % water suspension, Sigma Aldrich) to form an electrode consisting of 95 wt % active carbon material and 5 wt % binder. The electrode was rolled to a thickness of ~45 μm using a rolling mill, punched into ~1 cm diameter, and left to dry in an oven at 100 °C for 24 h. The typical mass loading on one electrode was 1.3 mg/cm^2 with an apparent electrode density of 0.59 g cm^{-3}. Thicker electrodes (~230 μm) were also prepared with a mass loading of 10.4 mg cm^{-2} and electrode density of 0.45 g cm^{-3}. The supercapacitors were assembled in a symmetrical two-electrode configuration, namely, a test cell consisting of two current collectors (Al foil with thin carbon coating layer, Exopack), two electrodes, and a porous separator (Celgard 3501) supported in a test fixture consisting of two stainless steel plates.[27] Ionic liquids of 1-butyl-3-methylimidazolium tetrafluoroborate, [BMIM][BF_4] (Sigma Aldrich), and 1-ethyl-3-methylimidazolium bis(trifluoromethylsulfonyl)imide, [EMIM][TFSI] (Boulder Ionics), were diluted in acetonitrile with a weight ratio of 1:1 and used as electrolytes.

Cyclic voltammetry, galvanostatic charge/discharge, and electrochemical impedance spectroscopy were carried out on a test cell with an asMEG-O electrode and ionic liquid electrolytes using an Autolab PESTAT302N potentiostat.

The gravimetric specific capacitance, C_{sp} (F g^{-1}), for a single electrode was calculated from each galvanostatic charge–discharge curve according to

$$C_{sp} = \frac{4I}{m\,dV/dt}$$

where I is the constant current, m is the total mass for both carbon electrodes, and dV/dt was calculated from the slope obtained by fitting a straight line to the discharge curve over the range V_{max} to (1/2)V_{max}.

The energy density was estimated by using the following formula and normalizing to the mass of the two carbon electrodes and the total mass of the cell.

$$E = \frac{1}{8} C_{sp} V_{max}^2$$

The effective series resistance was estimated using the voltage drop at the beginning of the discharge, V_{drop}, at certain constant current I, according to

$$R_{ESR} = \frac{V_{drop}}{2I}$$

The power density was calculated as

$$P = \frac{(V_{max} - V_{drop})^2}{4R_{ESR}m}$$

Characterization Methods. Scanning electron microscopy images were collected on a Hitachi S-4800 and also on a FEI Quanta-600, each operated at 30 kV. Transmission electron microscopy images were recorded on a JEOL JEM-2100F operated at 200 kV; the samples were dispersed in water and dropped on a holey carbon coated copper grid.

The N_2 adsorption and desorption isotherms were measured at 77 K on a Quantachrome Nova 2000, and the CO_2 isotherms were recorded at 273 K with a Micromeritics TriStar 3000. Prior to the gas sorption measurements, all the samples were outgassed in a vacuum at 120 °C for 24 h. The specific surface area and the pore size distribution were calculated using the Braunauer–Emmett–Teller (BET) method, and the relative pressure range of P/P_0 from 0.1 to 0.3 was used for multipoint BET calculations. Nonlocal density functional theory assuming the pores are slit/cylinder shaped was used to determine the pore size distribution and micropore and mesopore volume.

X-ray photoelectron spectroscopy was conducted with an ESCA2000 spectrometer using an Al Kα source (1486.6 eV photons) to analyze the chemical composition of the samples. Elemental analysis was done with a Flash EA1112 (CE) system (Thermo Scientific).

Conflict of Interest: The authors declare no competing financial interest.

Acknowledgment. We acknowledge support from the National Science Foundation (grant no. DMR-1206986).

Supporting Information Available: Additional experimental details and electrochemical analysis graphs. This material is available free of charge *via* the Internet at http://pubs.acs.org.

REFERENCES AND NOTES

1. Miller, J. R.; Simon, P. Materials Science - Electrochemical Capacitors for Energy Management. *Science* **2008**, *321*, 651–652.
2. Simon, P.; Gogotsi, Y. Materials for Electrochemical Capacitors. *Nat. Mater.* **2008**, *7*, 845–854.
3. Burke, A. R&D Considerations for the Performance and Application of Electrochemical Capacitors. *Electrochim. Acta* **2007**, *53*, 1083–1091.
4. Chmiola, J.; Yushin, G.; Gogotsi, Y.; Portet, C.; Simon, P.; Taberna, P. L. Anomalous Increase in Carbon Capacitance at Pore Sizes Less Than 1 Nanometer. *Science* **2006**, *313*, 1760–1763.
5. Kotz, R.; Carlen, M. Principles and Applications of Electrochemical Capacitors. *Electrochim. Acta* **2000**, *45*, 2483–2498.
6. Armand, M.; Endres, F.; MacFarlane, D. R.; Ohno, H.; Scrosati, B. Ionic-Liquid Materials for the Electrochemical Challenges of the Future. *Nat. Mater.* **2009**, *8*, 621–629.
7. Portet, C.; Lillo-Rodenas, M. A.; Linares-Solano, A.; Gogotsi, Y. Capacitance of KOH Activated Carbide-Derived Carbons. *Phys. Chem. Chem. Phys.* **2009**, *11*, 4943–4945.
8. Dash, R.; Chmiola, J.; Yushin, G.; Gogotsi, Y.; Laudisio, G.; Singer, J.; Fischer, J.; Kucheyev, S. Titanium Carbide Derived Nanoporous Carbon for Energy-Related Applications. *Carbon* **2006**, *44*, 2489–2497.
9. Xing, W.; Qiao, S. Z.; Ding, R. G.; Li, F.; Lu, G. Q.; Yan, Z. F.; Cheng, H. M. Superior Electric Double Layer Capacitors Using Ordered Mesoporous Carbons. *Carbon* **2006**, *44*, 216–224.
10. Jurewicz, K.; Vix-Guterl, C.; Frackowiak, E.; Saadallah, S.; Reda, A.; Parmentier, J.; Patarin, J.; Beguin, F. Capacitance Properties of Ordered Porous Carbon Materials Prepared by a Templating Procedure. *J. Phys. Chem. Solids* **2004**, *65*, 287–293.
11. Pekala, R. W.; Farmer, J. C.; Alviso, C. T.; Tran, T. D.; Mayer, S. T.; Miller, J. M.; Dunn, B. Carbon Aerogels for Electrochemical Applications. *J. Non-Cryst. Solids* **1998**, *225*, 74–80.
12. Futaba, D. N.; Hata, K.; Yamada, T.; Hiraoka, T.; Hayamizu, Y.; Kakudate, Y.; Tanaike, O.; Hatori, H.; Yumura, M.; Iijima, S. Shape-Engineerable and Highly Densely Packed Single-Walled Carbon Nanotubes and Their Application as Supercapacitor Electrodes. *Nat. Mater.* **2006**, *5*, 987–994.
13. Frackowiak, E.; Beguin, F. Electrochemical Storage of Energy in Carbon Nanotubes and Nanostructured Carbons. *Carbon* **2002**, *40*, 1775–1787.
14. Niu, C. M.; Sichel, E. K.; Hoch, R.; Moy, D.; Tennent, H. High Power Electrochemical Capacitors Based on Carbon Nanotube Electrodes. *Appl. Phys. Lett.* **1997**, *70*, 1480–1482.
15. Zhu, Y. W.; Murali, S.; Cai, W. W.; Li, X. S.; Suk, J. W.; Potts, J. R.; Ruoff, R. S. Graphene and Graphene Oxide: Synthesis, Properties, and Applications. *Adv. Mater.* **2010**, *22*, 3906–3924.
16. Stoller, M. D.; Park, S. J.; Zhu, Y. W.; An, J. H.; Ruoff, R. S. Graphene-Based Ultracapacitors. *Nano Lett.* **2008**, *8*, 3498–3502.
17. Zhu, Y. W.; Murali, S.; Stoller, M. D.; Velamakanni, A.; Piner, R. D.; Ruoff, R. S. Microwave Assisted Exfoliation and Reduction of Graphite Oxide for Ultracapacitors. *Carbon* **2010**, *48*, 2118–2122.
18. Liu, C. G.; Yu, Z. N.; Neff, D.; Zhamu, A.; Jang, B. Z. Graphene-Based Supercapacitor with an Ultrahigh Energy Density. *Nano Lett.* **2010**, *10*, 4863–4868.
19. Zhu, Y. W.; Murali, S.; Stoller, M. D.; Ganesh, K. J.; Cai, W. W.; Ferreira, P. J.; Pirkle, A.; Wallace, R. M.; Cychosz, K. A.; Thommes, M.; *et al.* Carbon-Based Supercapacitors Produced by Activation of Graphene. *Science* **2011**, *332*, 1537–1541.
20. Zhang, L. L.; Zhao, X.; Stoller, M. D.; Zhu, Y. W.; Ji, H. X.; Murali, S.; Wu, Y. P.; Perales, S.; Clevenger, B.; Ruoff, R. S. Highly Conductive and Porous Activated Reduced Graphene Oxide Films for High-Power Supercapacitors. *Nano Lett.* **2012**, *12*, 1806–1812.
21. El-Kady, M. F.; Strong, V.; Dubin, S.; Kaner, R. B. Laser Scribing of High-Performance and Flexible Graphene-Based Electrochemical Capacitors. *Science* **2012**, *335*, 1326–1330.
22. Wu, Z. S.; Sun, Y.; Tan, Y. Z.; Yang, S. B.; Feng, X. L.; Mullen, K. Three-Dimensional Graphene-Based Macro- and Mesoporous Frameworks for High-Performance Electrochemical Capacitive Energy Storage. *J. Am. Chem. Soc.* **2012**, *134*, 19532–19535.
23. Choi, B. G.; Yang, M.; Hong, W. H.; Choi, J. W.; Huh, Y. S. 3D Macroporous Graphene Frameworks for Supercapacitors with High Energy and Power Densities. *ACS Nano* **2012**, *6*, 4020–4028.
24. Luo, J. Y.; Jang, H. D.; Huang, J. X. Effect of Sheet Morphology on the Scalability of Graphene-Based Ultracapacitors. *ACS Nano* **2013**, *7*, 1464–1471.
25. Luo, J. Y.; Jang, H. D.; Sun, T.; Xiao, L.; He, Z.; Katsoulidis, A. P.; Kanatzidis, M. G.; Gibson, J. M.; Huang, J. X. Compression and Aggregation-Resistant Particles of Crumpled Soft Sheets. *ACS Nano* **2011**, *5*, 8943–8949.
26. Ravikovitch, P. I.; Vishnyakov, A.; Russo, R.; Neimark, A. V. Unified Approach to Pore Size Characterization of Microporous Carbonaceous Materials from N_2, Ar, and CO_2 Adsorption Isotherms. *Langmuir* **2000**, *16*, 2311–2320.

27. Stoller, M. D.; Ruoff, R. S. Best Practice Methods for Determining an Electrode Material's Performance for Ultracapacitors. *Energy Environ. Sci.* **2010**, *3*, 1294–1301.
28. Taberna, P. L.; Simon, P.; Fauvarque, J. F. Electrochemical Characteristics and Impedance Spectroscopy Studies of Carbon-Carbon Supercapacitors. *J. Electrochem. Soc.* **2003**, *150*, A292–A300.
29. Gogotsi, Y.; Simon, P. True Performance Metrics in Electrochemical Energy Storage. *Science* **2011**, *334*, 917–918.
30. Murali, S.; Quarles, N.; Zhang, L. L.; Potts, J. R.; Tan, Z.; Lu, Y.; Zhu, Y.; Ruoff, R. S. Volumetric Capacitance of Compressed Activated Microwave-Expanded Graphite Oxide (a-MEGO) Electrodes. *Nano Energy* **2013**, 10.1016/j.nanoen.2013.01.007.
31. Park, S.; An, J. H.; Piner, R. D.; Jung, I.; Yang, D. X.; Velamakanni, A.; Nguyen, S. T.; Ruoff, R. S. Aqueous Suspension and Characterization of Chemically Modified Graphene Sheets. *Chem. Mater.* **2008**, *20*, 6592–6594.